OXFORD

SOT | Society of Toxicology
www.toxsci.oxfordjournals.org

TOXICOLOGICAL SCIENCES, 143(1), 2015, 16–25

doi: 10.1093/toxsci/kfu206
Advance Access Publication Date: October 31, 2014

Synchrotron-Based Imaging of Chromium and γ-H2AX Immunostaining in the Duodenum Following Repeated Exposure to Cr(VI) in Drinking Water

Chad M. Thompson*,[1], Jennifer Seiter[†], Mark A. Chappell[†], Ryan V. Tappero[‡], Deborah M. Proctor[§], Mina Suh[§], Jeffrey C. Wolf[¶], Laurie C. Haws[||], Rock Vitale[|||], Liz Mittal*, Christopher R. Kirman[||||], Sean M. Hays[#], and Mark A. Harris*

*ToxStrategies, Inc., Katy, Texas 77494, [†]U.S. Army Engineer Research and Development Center, Vicksburg, Mississippi 39180, [‡]Photon Sciences Department, Brookhaven National Laboratory, Upton, New York 11973, [§]ToxStrategies, Inc., Mission Viejo, California 92692, [¶]Experimental Pathology Laboratories, Sterling, Virginia 20166, [||]ToxStrategies, Inc., Austin, Texas 78731, [|||]Environmental Standards, Inc., Valley Forge, Pennsylvania 19482, [||||]Summit Toxicology, LLP, Orange Village, Ohio 44022 and [#]Summit Toxicology, LLP, Allenspark, Colorado 80510

[1]To whom correspondence should be addressed at ToxStrategies, Inc., 23123 Cinco Ranch Blvd., Suite 220, Katy, Texas 77494; Fax: 832-218-2756. E-mail: cthompson@toxstrategies.com

ABSTRACT

Current drinking water standards for chromium are for the combined total of both hexavalent and trivalent chromium (Cr(VI) and Cr(III)). However, recent studies have shown that Cr(III) is not carcinogenic to rodents, whereas mice chronically exposed to high levels of Cr(VI) developed duodenal tumors. These findings may suggest the need for environmental standards specific for Cr(VI). Whether the intestinal tumors arose through a mutagenic or non-mutagenic mode of action (MOA) greatly impacts how drinking water standards for Cr(VI) are derived. Herein, X-ray fluorescence (spectro)microscopy (μ-XRF) was used to image the Cr content in the villus and crypt regions of duodena from B6C3F1 mice exposed to 180 mg/l Cr(VI) in drinking water for 13 weeks. DNA damage was also assessed by γ-H2AX immunostaining. Exposure to Cr(VI) induced villus blunting and crypt hyperplasia in the duodenum—the latter evidenced by lengthening of the crypt compartment by ∼2-fold with a concomitant 1.5-fold increase in the number of crypt enterocytes. γ-H2AX immunostaining was elevated in villi, but not in the crypt compartment. μ-XRF maps revealed mean Cr levels >30 times higher in duodenal villi than crypt regions; mean Cr levels in crypt regions were only slightly above background signal. Despite the presence of Cr and elevated γ-H2AX immunoreactivity in villi, no aberrant foci indicative of transformation were evident. These findings do not support a MOA for intestinal carcinogenesis involving direct Cr-DNA interaction in intestinal stem cells, but rather support a non-mutagenic MOA involving chronic wounding of intestinal villi and crypt cell hyperplasia.

Key words: hexavalent chromium; Cr(VI); synchrotron; duodenum; carcinogenesis; mode of action; H2AX

Chromium from natural and anthropogenic sources is present in drinking water primarily in trivalent (Cr(III)) and hexavalent (Cr(VI)) forms (Ellis *et al.*, 2002; McNeill *et al.*, 2012; Oze *et al.*, 2007; U.S. EPA, 2014). The current U.S. maximum contaminant level (MCL) for total Cr is 0.1 mg/l (U.S. EPA, 1991), and is based on the absence of toxicity observed in rats chronically exposed to Cr(VI) in drinking water for 1 year (Mackenzie *et al.*, 1958; U.S. EPA, 1998). More recent 2-year bioassays conducted by the National Toxicology Program (NTP) found that although Cr(III) was not carcinogenic to rodents (NTP, 2008a; Stout *et al.*, 2009b), B6C3F1 mice exposed to ≥20 mg/l Cr(VI) in drinking water developed adenomas and carcinomas of the duodenum and jejunum (NTP, 2008b; Stout *et al.*, 2009a). Considering that these carcinogenic concentrations are ~20,000 times higher than average Cr(VI) concentrations in U.S. drinking water (~0.001 mg/l) (McNeill *et al.*, 2012; U.S. EPA, 2014), and that ≤10 mg/l Cr(VI) was not carcinogenic to mice (NTP, 2008a; Stout *et al.*, 2009b), it is important to understand the health hazards posed by environmentally relevant levels of Cr(VI) in drinking water.

When ingested, Cr(VI) is reduced to Cr(III) by saliva and gastric fluid or taken into cells along the gastrointestinal tract through anion transporters (De Flora, 1978, 1997; Kirman *et al.*, 2013; Proctor *et al.*, 2012). Cr(III) absorption, in contrast, is not transporter mediated and thus its absorption and toxicity is minimal (NTP, 2008a; Stout *et al.*, 2009b). Intracellular reduction of Cr(VI) to Cr(III) can generate reactive oxygen species and Cr(III)-ligands that can damage cellular constituents such as proteins and DNA (De Flora, 1978; Nickens *et al.*, 2010; O'Brien *et al.*, 2003). As chromium can interact with DNA, some scientists have concluded that the intestinal tumors observed in mice must be the result of a mutagenic mode of action (MOA) (McCarroll *et al.*, 2010; Zhitkovich, 2011). However, recent studies relying more heavily on data obtained from the target tissue of interest (i.e. duodenum) provide strong support for a MOA involving chronic damage to the intestinal mucosa (Thompson *et al.*, 2013). Specifically, Cr(VI) exposure to B6C3F1 mice causes villous cytotoxicity, followed by crypt proliferation without evidence of cytogenetic damage or increases in *kras* mutation frequency (O'Brien *et al.*, 2013; Thompson *et al.*, 2011). Rats chronically exposed to the same high concentrations of Cr(VI) in drinking water did not develop villus damage, crypt proliferation, or intestinal tumors (NTP, 2008b; Stout *et al.*, 2009a).

The pattern of Cr(VI)-induced lesions in mice is consistent with the fact that most dietary absorption occurs via villus enterocytes of the duodenum and proximal jejunum (DeSesso and Jacobson, 2001). Villus enterocytes are differentiated, short-lived, and destined to slough into the intestinal lumen, and therefore DNA damage in villus enterocytes poses little, if any, carcinogenic risk (Potten and Loeffler, 1990). In contrast, the long-lived pluripotent stem cells of the intestine reside below the mucosal surface in the lower portions of the intestinal crypts (Figure 1). Crypt stem cells harboring mutations in proto-oncogenes like *kras* are thought to be the source of intestinal adenomas and carcinomas (Barker *et al.*, 2009; Rizk and Barker, 2012). Whether the mutations that eventually give rise to tumors occur as a result of direct Cr-DNA interaction in crypt stem cells or increased cell proliferation due to chronic mucosal injury has a significant impact on the appropriate approach for low-dose extrapolation in risk assessment. Risk assessment approaches relying on linear low-dose extrapolation result in health-based screening levels <0.0001 mg/l (OEHHA, 2011; U.S. EPA, 2013), which are more than 10 times lower than average concentrations in the U.S. drinking water supply (McNeill *et al.*, 2012; U.S. EPA, 2014).

To further assess the MOA for mouse intestinal tumors and appropriate risk assessment approaches, herein we examined the distribution of chromium, markers of DNA damage (phosphorylated H2AX, γ-H2AX), and changes in histopathology in the crypts and villi of duodenal tissues from mice exposed to carcinogenic concentrations of Cr(VI) in drinking water for 13 weeks. The results provide further evidence that the MOA involves a non-genotoxic, chronic wounding and healing mechanism associated with high Cr(VI) exposure that can be prevented by mitigating chronic exposures to high concentrations of Cr(VI) that damage the intestinal mucosa.

MATERIALS AND METHODS

Animals and study design. The NTP previously conducted 13-week and 2-year drinking water bioassays with Cr(VI), in the form of sodium dichromate dihydrate (SDD), in B6C3F1 mice and Fisher 344/N (F344) rats (NTP, 2007, 2008b; Stout *et al.*, 2009a). We subsequently conducted 13-week studies in B6C3F1 mice and F344 rats to better understand the MOA of Cr(VI)-induced tumors (Thompson *et al.*, 2011, 2012b). To minimize study variability for comparison with the NTP Cr(VI) studies, the in-life portion of our studies were conducted at the same research facility where the NTP studies were conducted, viz. Southern Research Institute (Birmingham, AL). Our overall study design was informed by the NTP studies, as well as an independent expert panel convened by Toxicology Excellence for Risk Assessment (http://www.tera.org/Peer/ Chromium/Chromium.htm). The analyses in this study were conducted on tissue samples from our two aforementioned 13-week studies (Thompson *et al.*, 2011, 2012b).

Complete details on the test substance, animal husbandry, and study design have been described in detail elsewhere (Thompson *et al.*, 2011, 2012b). Briefly, only female rodents were used in this study because males and females of each species responded similarly to Cr(VI) in the NTP studies (NTP, 2007, 2008b; Stout *et al.*, 2009a). Female B6C3F1 mice obtained from Charles River (Raleigh, NC) were exposed to 0.3, 4, 14, 60, 170, and 520 mg/l SDD (Sigma-Aldrich, Inc. Milwaukee, WI) in tap water; these values are equivalent to ~0.1, 1.4, 5, 20, 60, and 180 mg/l Cr(VI). Female F344 rats obtained from Charles River (Stone Ridge, NY) were exposed to the same concentrations with the exception that the 5 mg/l Cr(VI) group was omitted. These doses were similar to those used in the NTP 2-year bioassay (NTP, 2008b; Stout *et al.*, 2009a) with the exception that we included two additional, more environmentally relevant, dose groups (0.1 and 1.4 mg/l Cr(VI)). Dose formulations were analyzed in accordance with EPA Method SW-7196A and used only if concentrations were within ±10% of target concentrations.

The mice were ~4–5 weeks of age when they arrived, were allowed to acclimate for ~2 weeks, and weighed 13.3–22.9 g at the start of the study. The rats were ~4 weeks of age when they arrived, were allowed to acclimate for ~2 weeks, and weighed 83.1–126.4 g at the start of the study. All animals were allowed *ad libitum* access to irradiated NTP-2000 chow (Zeigler Bros., Gardners, PA). All animal care conformed to the Guide for the Care and Use of Laboratory Animals, the U.S. Department of Agriculture through the Animal Welfare Act (Public Law 99-198) and to the applicable SOPs of Southern Research Institute.

Histopathology. At study termination, 10 animals per dose group were sacrificed for histopathological examination. Rodents

were euthanized by CO_2 asphyxiation and subjected to a complete gross examination at the time of necropsy. The oral cavity, duodenum, and jejunum were collected from each rodent and fixed in 10% neutral-buffered formalin. The duodenal specimens from B6C3F1 mice were 9.2 ± 0.6 cm, whereas duodenal specimens from F344 rats were 5.6 ± 0.7 cm. All duodenal analyses were at the approximate middle of the duodenum. Fixed tissues were trimmed, processed, and sectioned to ~5 μm, mounted on glass slides, and stained with hematoxylin and eosin (H&E) for microscopic examination.

Assessment of crypt length and crypt cell number in B6C3F1 mice. Preparation of duodenal sections for crypt length and number of enterocytes has been described in detail elsewhere (O'Brien *et al.*, 2013). In brief, paraffin-embedded 5-μm duodenal sections (3 per mouse) were stained for DNA using Feulgen's stain and analyzed by Experimental Pathology Laboratories, Inc. (EPL®; Sterling, VA). Ten full-length crypts were selected impartially in duodenal sections from 5 animals in each dose group. All sections were measured in a blinded fashion. Using image analysis software (Image-Pro® Plus, Media Cybernetics, Silver Spring, MD), all enterocytes from the selected crypts were individually marked and counted, and calibrated linear measurements were obtained of each crypt length.

Scoring of γ-H2AX immunoreactivity in B6C3F1 mice. Unstained 5-μm duodenal sections (1 per animal; 5 animals per group) were stained immunohistochemically for the γ-H2AX antigen with primary rabbit polyclonal γ-H2AX antibody (Abcam, ab2893) and secondary goat anti-rabbit antibody (Vector, BA-6100) using routine avidin-biotin complex (ABC) methodology (Vector, PK-6100) and a diaminobenzidine (DAB) chromagen (Biocare Medical, BDB2004H). An American College of Veterinary Pathologists board-certified veterinary pathologist scored crypt and villus areas individually for the presence of nuclear and/or cytoplasmic staining according to the following grading scale: Grade 0 = staining essentially not apparent; Grade 1 = mild amount of staining; Grade 2 = moderate amount of staining; Grade 3 = abundant staining (no samples exhibited abundant staining; therefore, this last category was not utilized). Results were confirmed by blinded review.

X-ray fluorescence microspectroscopy. Three serial sections were microtomed from the duodena of two mice each from the control and high-dose groups, as well as from one rat from the control and high-dose groups. One section (5 μm) was acquired for H&E staining, and two sections (20 μm) were obtained for synchrotron analysis. Sections for synchrotron analysis were placed on Mylar film. Synchrotron-based micro-X-ray fluorescence (μ-XRF) was performed at beamline X27A at the National Synchrotron Light Source at Brookhaven National Laboratory in Upton, NY. The beam size on the sample was ~7 μm × 10 μm using Rh-coated Kirkpatrick-Baez focusing optics. X-rays were selected using a water-cooled channel-cut Si(111) monochromator. For XRF and XANES analysis, the monochromator was calibrated using a Chromium foil to the Cr K-edge (5989 eV), and additional XRF imaging was performed at 6.2 and 11keV. XRF data were collected using a Vortex ME4 Silicon Drift Detector Array. The μ-XRF maps were analyzed and generated using the X27A beamline software (Figure 1).

Elemental detection by XRF analysis is established by comparison with a threshold, or a limit of detection, which is the combination of the mean background intensity and the background noise. The instrument detection limit (IDL) represents a

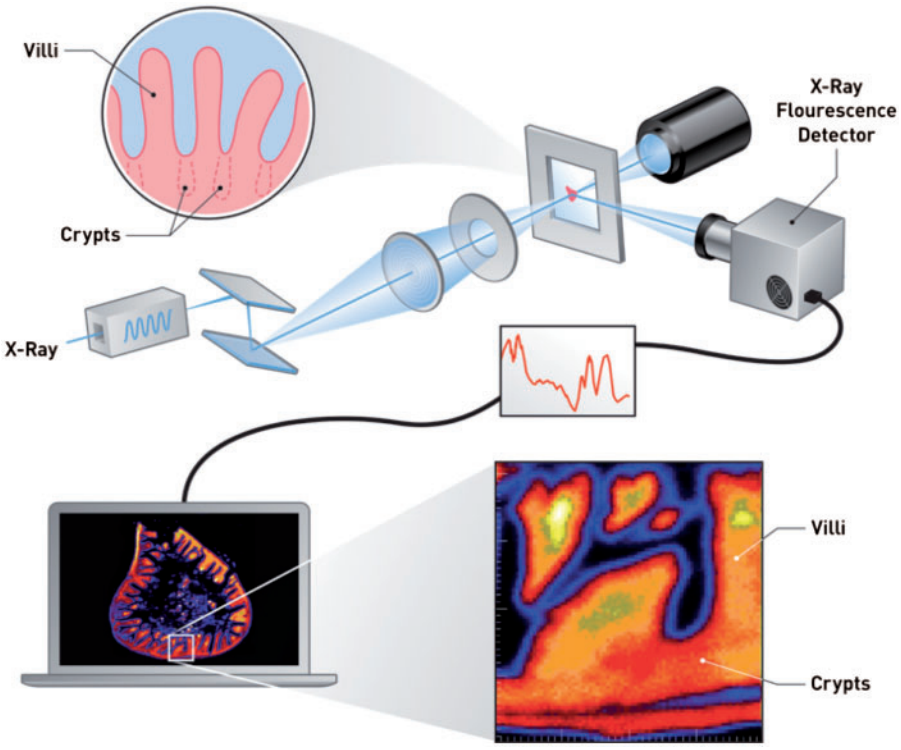

FIG. 1. Overview of X-ray fluorescence mapping and the small intestine. An incident X-ray beam is focused on a formalin-fixed, paraffin-embedded intestinal section. Raster-scanning across the specimen yields elemental X-ray fluorescence (XRF) maps for elements of interest (see computer screen). The top inset (circle) depicts the intestinal villi with crypt invaginations depicted as dotted lines. The bottom inset (square) shows a magnified version of the intestinal mucosa containing a crypt region residing below the space between two villi.

threshold above which peak intensity can be distinguished from the background intensity and noise at a specified level of confidence. Under this threshold the peak intensity is assumed to be indistinguishable from the background noise. In XRF analysis, concentration is thus calculated from the difference between the measured peak intensity and the background intensity (Rousseau, 2001). The IDL is a minimum detection limit with a 99.95% confidence level to distinguish a net intensity from background—if the net intensity is 4.65σ above the mean background intensity. Using equations found in Rousseau (2001), an IDL for Cr in these samples was established to be 0.15 μg/g (0.15 ppm). This value is consistent with previous studies indicating detection limits for the microprobe typically vary between 0.1 and 10 ppm depending on the element and the matrix analyzed (Lanzirotti and Sutton, 2002). The practical limit of quantification (PQL) is defined herein as 5 times the IDL, viz. 0.75 μg/g. For Cr quantification, XRF maps were averaged and total Cr levels were determined for 24 intact villi and 24 crypts. Background levels were measured by taking 24 readings adjacent to the duodenal tissue (i.e., paraffin and Mylar only) embedded in the 20-μm section.

Statistical evaluations. Data were analyzed by one-way ANOVA followed by Dunnett's tests using Prism 6 for Mac (GraphPad Software, San Diego, CA, www.graphpad.com). Threshold dose-response analysis using smoothing spline and bilinear modeling was conducted using the R (http://www.R-project.org) package *drsmooth* (Hixon and Bichteler, 2013).

RESULTS

Assessment of DNA Damage and Crypt Morphology in the Mouse Duodenum

Previous studies have shown that undifferentiated proliferating intestinal cells are more prone to Cr(VI)-induced DNA damage (e.g., H2AX phosphorylation) than differentiated intestinal cells *in vitro* (Thompson *et al.*, 2012a). To examine DNA damage *in vivo*, duodenal sections taken from mice exposed to tap water or 180 mg/l Cr(VI) for 13 weeks were stained for γ-H2AX. Sections from treated mice exhibited blunted villi and elongated crypts (Figure 2A and B; Supplementary Figure S1). Both treated and untreated mice exhibited slight amounts of finely stippled gray-brown γ-H2AX immunostaining of mucosal epithelial nuclei. Similar nuclear staining was observed in leukocytes within the mucosal lamina propria, smooth muscle myocytes, and in portions of adjacent exocrine pancreas. Finely stippled staining was more prevalent in epithelial cells of crypts than villi. Immunostaining of the villus epithelium and lamina propria was increased slightly in treated mice (Table 1), and all sections from treated mice exhibited regional positive staining in the lamina propria of the villus tips (Figure 2A and B insets). This staining appeared to be contained primarily within the distended cytoplasm of histiocytic macrophages—possibly as a result of γ-H2AX protein scavenged from damaged mucosal epithelial cells that were subsequently exfoliated into the lumen. In duodenal samples from both treated and control mice, individual crypt epithelial cells had punctate staining of the nuclear and cytoplasmic regions, which appeared to preferentially involve dividing and exfoliating cells. Overall, the γ-H2AX staining of crypts on a cell-by-cell basis was similar in treated and untreated mice (Figure 2C and D; Table 1). As there were no indications of increased γ-H2AX immunostaining of crypts in the high-dose group, immunostaining was not conducted for lower doses groups.

At low magnification, γ-H2AX immunostaining in the crypt region appears darker in the treated mouse specimens (Figure 2B); however, this appearance is due to the increased cellular density caused by crypt epithelial proliferation. The crypts of mice exposed to 180 mg/l Cr(VI) are visibly taller (Fig. 2C and D) than those of untreated mice (190.5 ± 28.4 vs 98.3 ± 17.1 μm; $P \leq .0001$; Fig. 2E), and there was an increase in the number of crypt enterocytes visible in cross-sections (63.9 ± 11.9 vs 38.4 ± 2.6, $P \leq .0001$; Figure 2F). The crypt lengths and number of crypt enterocytes in cross-section for the other dose groups are shown in Supplementary Tables S1 and S2. Dose-response modeling of these two crypt metrics with the *R* package *drsmooth* (Hixon and Bichteler, 2013) indicated potential thresholds ranging from 2.3 to 4.5 mg/l Cr(VI) (Supplementary Figure S2 and Supplementary Table S3).

Imaging of Chromium in the Mouse Duodenum

The absence of increased γ-H2AX staining in the proliferative crypt compartment of mice exposed to Cr(VI) suggests that Cr(VI) does not directly reach crypt enterocytes *in vivo*. To more directly examine whether Cr(VI) reaches the crypt compartment, μ-XRF was used to determine the localization and abundance of Cr and other elements in duodenal sections of mice exposed to 0 or 180 mg/l Cr(VI) in drinking water for 13 weeks. The μ-XRF maps exhibited strong calcium (Ca) and sulfur (S) signals in the crypts and villi (effectively outlining the shape of the small intestine), whereas Cr signal (determined to be Cr(III)) was limited to the intestinal villi (Figure 3A). Magnification of the crypt-villus unit revealed contiguous signal for Ca and S, whereas there was a clear diminution of Cr signal in the crypt (Figure 3B). A similar pattern was observed in a duodenal section from another mouse exposed to 180 mg/l Cr(VI) (Supplementary Figure S3). Quantification of the μ-XRF map indicated that the mean and median concentrations of Cr in the villi were 14.0 and 11.9 μg/g, respectively, whereas the mean and median concentration of Cr in the crypt region was 0.4 and 0.4 μg/g (Figure 3C and D). Notably, the highest concentrations were detected near villus tips, with a maximal level detected of 96 μg/g. Chromium treatment did not appear to dramatically alter the μ-XRF maps for Ca and S (Figure 4); however, these maps clearly show the villus blunting in the duodena of treated animals.

Assessment of Aberrant Villous Foci in the Mouse Duodenum

Although it is generally believed that intestinal tumors arise from mutations in crypt stem cells, it was recently shown that aberrant crypt-like foci (visible by H&E stain) containing de-differentiated enterocytes expressing stem cell markers could be conditionally generated in the villi of genetically engineered mice (Schwitalla *et al.*, 2013). Considering that we have shown that both γ-H2AX staining and Cr are detected in villi at carcinogenic doses, duodenal villi were examined for the presence of aberrant foci. No aberrant foci were observed in duodenal H&E stained sections from control mice or mice exposed to 0.1–180 mg/l Cr(VI) for 13 weeks (Supplementary Table S4).

Imaging of Chromium in the Rat Duodenum

F344 rats did not exhibit villus blunting, crypt hyperplasia, or develop intestinal tumors in the 13-week and 2-year NTP studies (NTP, 2007, 2008b; Stout *et al.*, 2009a); therefore, γ-H2AX immunostaining, crypt metrics, and analysis of aberrant foci were not conducted in rats in this study. However, as we reported in Thompson *et al.* (2012), F344 rats in our 13-week study exhibited non-neoplastic lesions in the small intestine that were similar, albeit milder, to those observed in mice (Supplementary Figure S4; see "Discussion" section).

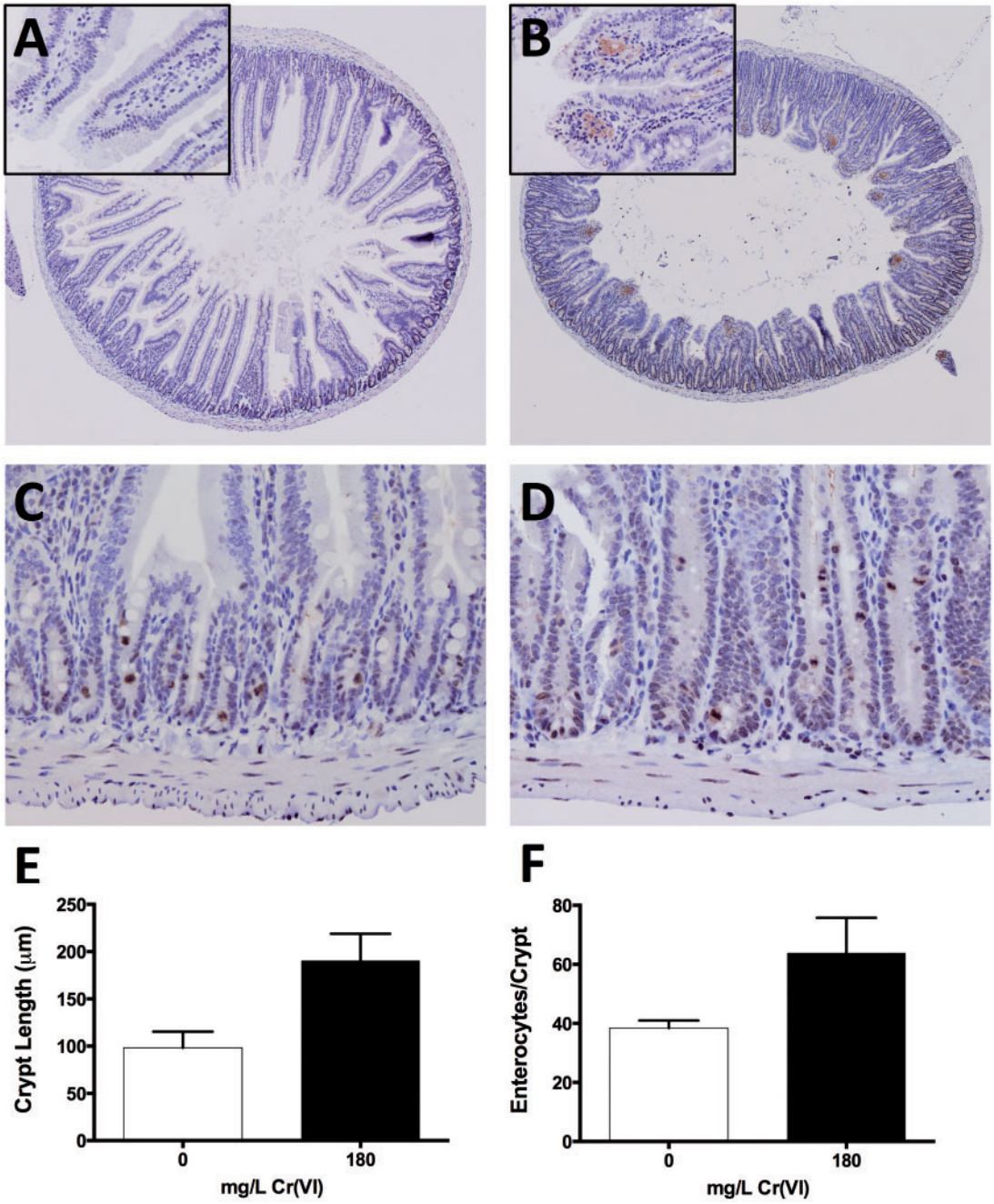

FIG. 2. Immunostaining of γ-H2AX in B6C3F1 duodenal sections. **A**, Representative duodenal section (4× objective) from control B6C3F1 mouse stained with anti γ-H2AX. **B**, Representative duodenal section (4× objective) from B6C3F1 mouse exposed to 180 mg/l Cr(VI) for 13 weeks, stained with anti γ-H2AX. Note the relative blunting of villi and expansion of the crypt compartment (crypt epithelial hyperplasia). Insets are magnifications (40×) of villi; γ-H2AX staining can be seen in the villi of treated mice only. **C**, Representative duodenal crypts (40× objective) from a control B6C3F1 mouse stained with anti γ-H2AX. **D**, Representative duodenal crypts (40× objective) from a mouse exposed to 180 mg/l Cr(VI) for 13 weeks, stained with anti-γ-H2AX. Images A–D were counterstained with hematoxylin. **E**, Duodenal crypt lengths differed between treated and untreated mice (*$P < .001$; Student's two-tailed *t* test; mean ± SD from 5 animals, 10 fully intact crypts measured per animal). **F**, Number of enterocytes per cross-section of crypt differed between treated and untreated mice (*$P < .01$; Student's two-tailed *t* test; mean ± SD from 5 animals, enterocyte counts from 10 fully intact crypts per animal).

Therefore, we conducted μ-XRF imaging in one of our rats exposed to 180 m/l Cr(VI) for 13 weeks to examine the distribution of Cr in the duodenum. Similar to mice, Cr was localized to the villi, and magnification of the crypt-villus unit revealed contiguous signal for Ca and S, but not Cr (Figure 5). Quantification of the μ-XRF map indicated mean and median concentrations in villi of 5.0 and 4.2 μg Cr/g.

DISCUSSION

We have previously shown that mice exposed to ≤180 mg/l Cr(VI) for 1 and 13 weeks did not show elevations in duodenal crypt micronuclei, nor increases in *kras* mutation frequency in scraped duodenal mucosa after 13 weeks of exposure (O'Brien *et al.*, 2013). Herein, we further assessed crypt health by staining

for phosphorylated H2AX (γ-H2AX), which is a sensitive indicator of DNA damage but can also be elevated during apoptosis (Bonner *et al.*, 2008; Kinner *et al.*, 2008). Increased immunoreactivity was observed in the duodenal villi—primarily in histiocytes—possibly as a result of cellular and protein scavenging.

TABLE 1. Scoring of γ-H2AX Immunoreactivity

Cr(VI), mg/l	Animal no.	Crypt epithelium	Villus epithelium	Lamina propria of villus tip
0	6	2	0	0
0	7	2	0	0
0	8	2	0	0
0	9	2	0	0
0	10	2	0	0
180	482	2	1	2
180	483	2	0	2
180	484	2	1	2
180	485	2	1	2
180	486	2	2	2

However, the increased villous γ-H2AX staining could also be due to increases in apoptosis we previously observed in the lamina propria of mice exposed to high concentrations of Cr(VI) (Thompson *et al.*, 2011). The negative findings in the crypt with respect to γ-H2AX staining were strengthened by the synchrotron analyses indicating little if any Cr is present in the crypt region of mice. Specifically, the levels in the crypt region were above the IDL but below the PQL; and moreover were ~37-fold lower than the villi. A similar pattern of Cr distribution was observed in the rat duodenum. The low Cr signal detected in the crypt region of these samples may reflect Cr present in vasculature, as we previously showed elevated Cr levels in plasma of mice and rats exposed to ≥20 mg/l Cr(VI) (Kirman *et al.*, 2012).

Considering the evidence against Cr directly affecting the stem cells of the crypt compartment, it is perhaps reasonable to consider whether the presence of Cr in duodenal villi could lead to tumors through a mutagenic MOA. However, the presence of Cr in intestinal villi should pose little carcinogenic risk because villus enterocytes are differentiated cells destined to slough into the lumen within a few days (Potten and Loeffler, 1990). In fact, even the proliferating daughter cells in the transit amplifying region of the crypt lack markers of "stemness" (Barker *et al.*, 2009; Schuijers and Clevers, 2012; van der Flier and Clevers, 2009).

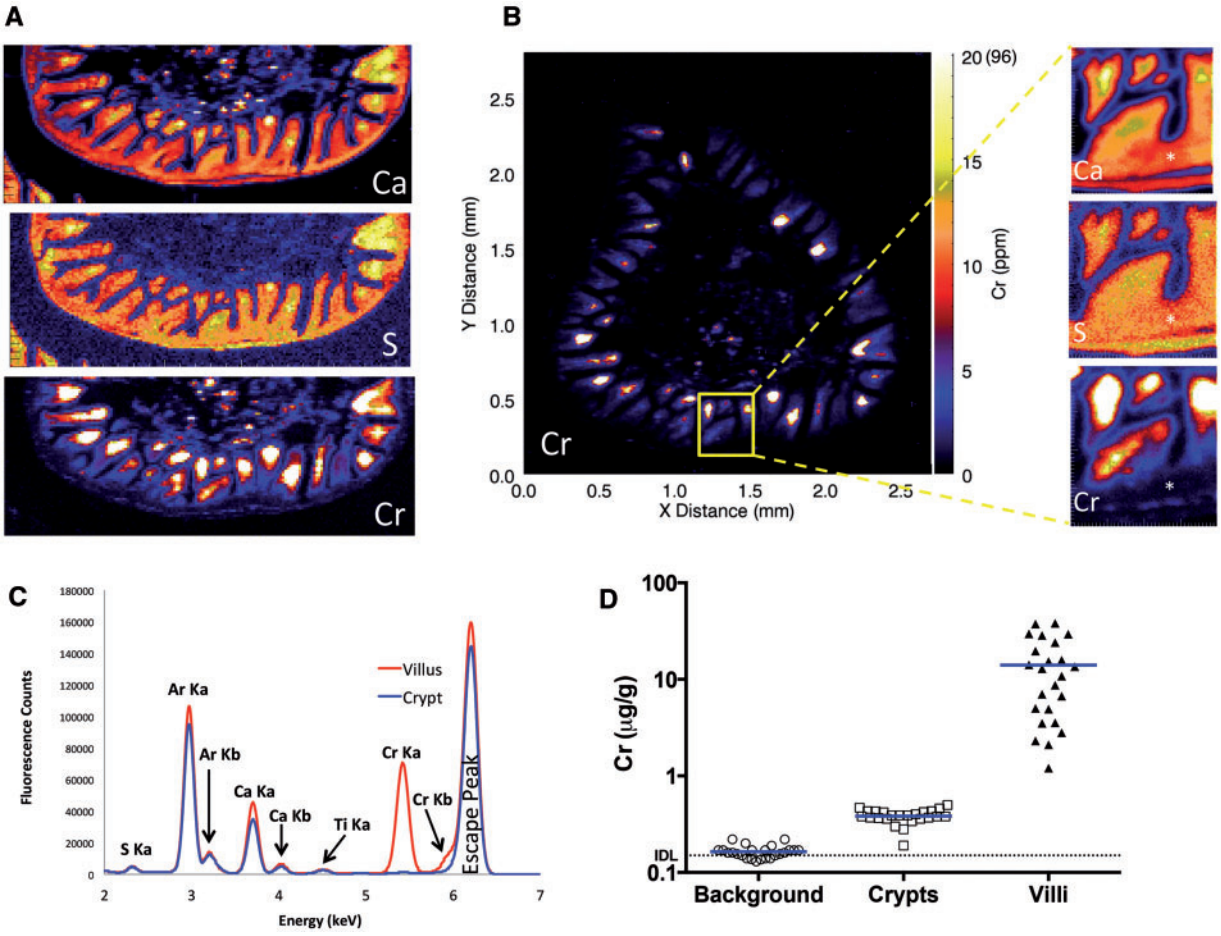

FIG. 3. XRF (X-ray fluorescence) maps in a representative duodenal section from a mouse exposed to 180 mg/l Cr(VI) for 13 weeks. **A**, XRF maps for Ca, S, and Cr in same intestinal section. **B**, XRF Cr map for transverse duodenal section (left) with magnified images of crypt (asterisk) and villus signal in the same intestinal section. Note: the scale for the larger Cr XRF map is in micro-gram per gram, whereas scales for magnified images are in fluorescence counts (i.e., different units). The white color indicates Cr concentrations ≥20 μg/g; the maximal level detected is shown in parentheses (96 μg/g). **C**, Representative multi channel array plot depicting fluorescence (Ka and Kb) emission lines for the villus and crypt regions of a duodenal section from a mouse exposed to Cr(VI). **D**, Comparison of the average Cr signal from 24 crypts, villi, and background (non-tissue) areas from 3B (mean indicated by blue lines). The instrument detection limit (IDL), 0.15 μg/g is indicated by the dotted line. The practical limit of quantification (PQL) is 0.75 μg/g (5× IDL).

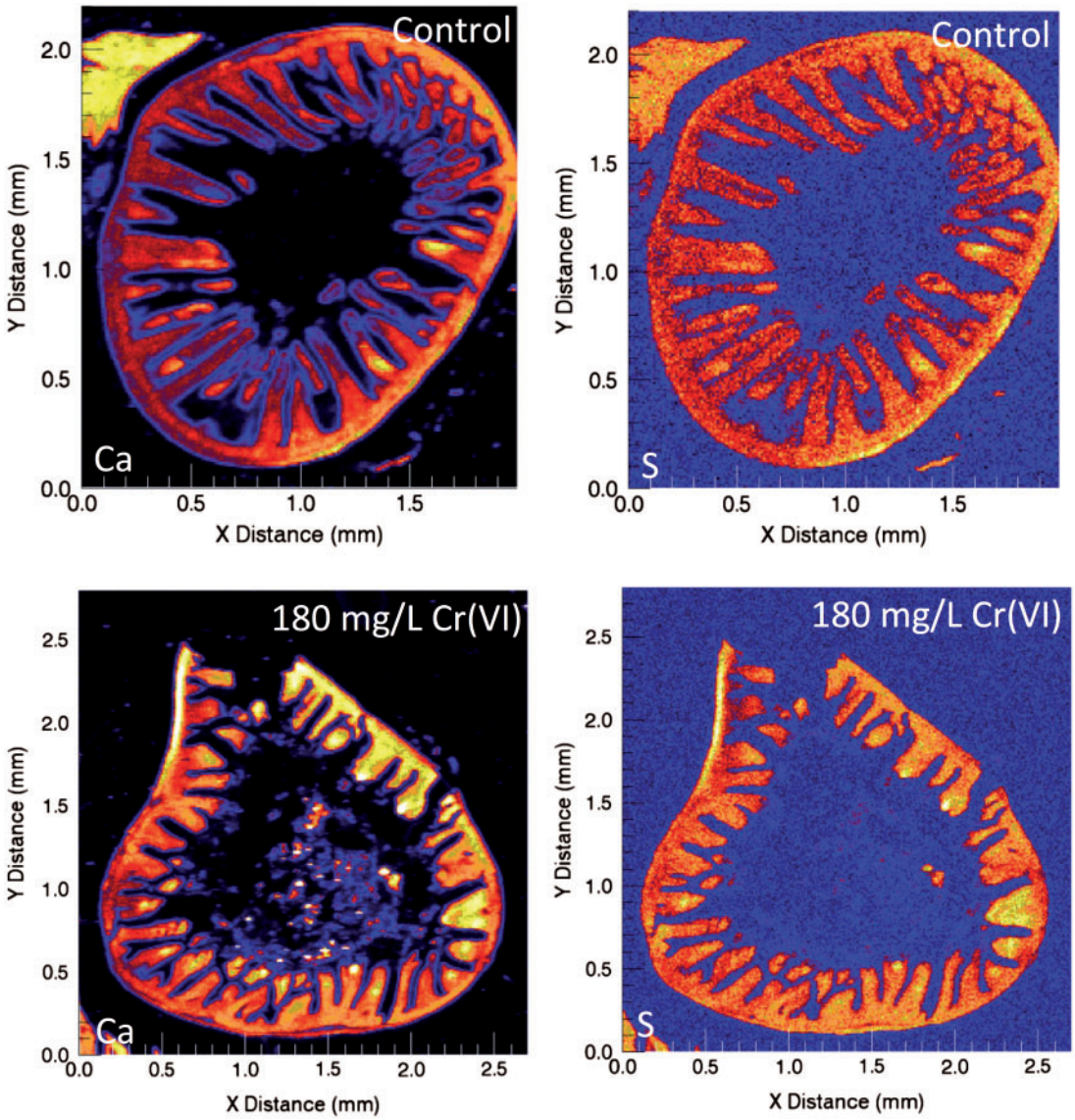

FIG. 4. XRF (X-ray fluorescence) maps for Ca and S in duodenal sections from mice exposed to 0 or 180 mg/l Cr(VI) for 13 weeks. Note the villus blunting evident in treated samples. Note: XRF maps for Cr are not shown because there was no discernible image in untreated mice.

However, genetically engineered mice harboring dual activating mutations in both Wnt/β-catenin and NF-κB signaling pathways can be coaxed into expressing genes that confer stemness; and these reprogrammed/de-differentiated villous enterocytes can form crypt-like foci on villi (Schwitalla *et al.*, 2013). Importantly, no such foci were observed in the present study, nor in other Cr(VI) drinking water studies (NTP, 2007, 2008b; Stout *et al.*, 2009a). Although it is conceivable that inflammatory-mediated TNF-α/NF-κB signaling might cooperate with mutations in the Wnt/β-catenin pathway to promote villus de-differentiation without the need for activating mutations in the NF-κB pathway, chronic inflammation has not been observed in the mouse duodenum in either the 13-week or 2-year Cr(VI) bioassays (NTP, 2007, 2008b; Stout *et al.*, 2009a; Thompson *et al.*, 2011). Moreover, TNF-α protein and transcript levels were not elevated in the mouse duodenum after 13 weeks of exposure to ≤180 mg/l Cr(VI) (Kopec *et al.*, 2012; Thompson *et al.*, 2011). Considering further that rats in the NTP 2-year bioassay absorbed Cr (presumably via the intestine) as evidenced by Cr levels in blood, liver, and kidney (intestinal tissues were not analyzed) (NTP, 2008b), the presence of Cr in villi did not induce intestinal tumors. Thus, Cr does not appear to cause de-differentiation of committed villous enterocytes.

If Cr(VI) does not directly affect the crypt compartment, and reprogramming of committed villous enterocytes is unlikely, then the most plausible explanation for the Cr(VI)-induced tumors in mice is related to the increase in crypt hyperplasia. In fact, several authors have noted that proliferative responses in subchronic studies are predictive of longer-term cancer outcomes (Cohen, 2010; Gaylor, 2005). In the case of Cr(VI), the proliferative effects observed in intestines of mice in the subchronic NTP study (NTP, 2007) were predictive of tumor outcome in the chronic NTP bioassay (NTP, 2008b; Stout *et al.*, 2009a). This supports the idea that chronic proliferative pressure increased the probability of tumor formation. It has been suggested that chronic wounding and proliferation leads to an increase in the stem cell population of a tissue (Greenfield *et al.*, 1984). Considering that each stem cell division has some small

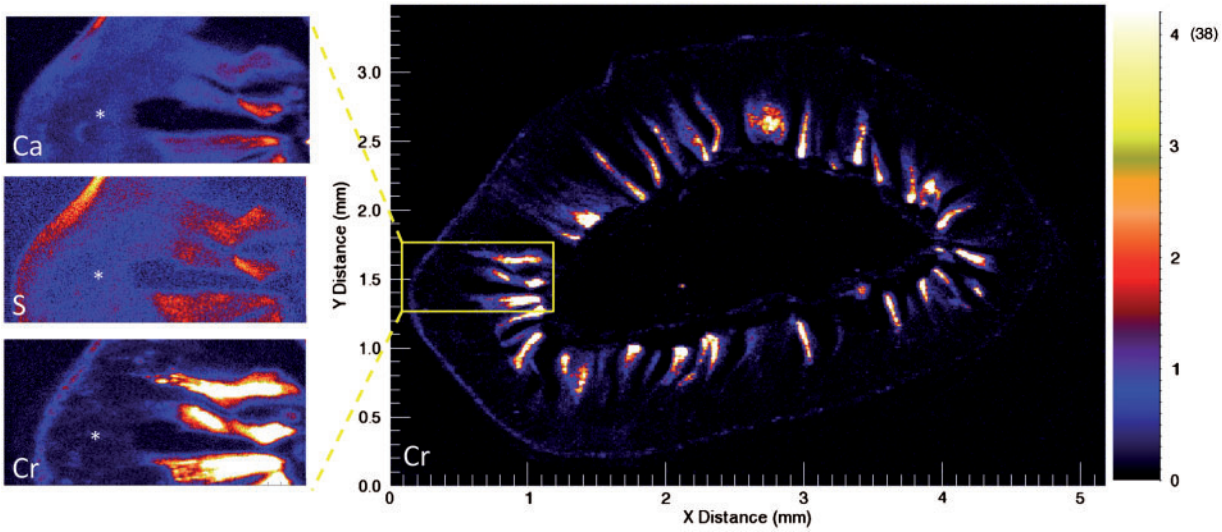

FIG. 5. XRF (X-ray fluorescence) maps in a representative duodenal section from a rat exposed to 180 mg/l Cr(VI) for 13 weeks. XRF Cr map for transverse duodenal section (right) with magnified images of crypt (asterisk) and villus signals for Ca, S, and Cr in the same intestinal section on the left. Note: the scale for the larger Cr XRF map is in micro-gram per gram, whereas scales for magnified images are in fluorescence counts. The white color indicates Cr concentrations ≥4 μg/g; the maximal level detected is shown in parentheses (38 μg/g).

probability of initiation or transformation (Greenfield *et al.*, 1984; Moolgavkar and Knudson, 1981), chronic wounding increases the probability of transformation over time. In this regard, we previously showed that 180 mg/l Cr(VI) increased crypt hyperplasia in the duodenum of mice after only 1 week of exposure—indicating a significant lifetime increase in crypt proliferation (Thompson *et al.*, 2011). Herein, we clearly showed that high concentrations of Cr(VI) increase the number of crypt enterocytes and length of the crypt compartment after 13 weeks of exposure. This is likely a result of an increased stem cell population giving rise to more daughter cells in the crypt. Finally, it should be pointed out that villous damage/blunting and crypt hyperplasia is an accepted MOA for other small intestinal carcinogens such as captan and folpet (Cohen *et al.*, 2010; Gordon, 2007; U.S. EPA, 2004).

Unlike F344 rats in the NTP study (NTP, 2007, 2008b), F344 rats in our 13-week study (Thompson *et al.*, 2012b) exhibited villous toxicity and crypt hyperplasia in the duodenum. The rats were obtained from different vendors, and the volume of water and test article consumed per day differed in the studies by nearly 2-fold (Supplementary Figure S5)—generally falling at opposite ends of reported ranges for normal intake. The μ-XRF maps for Cr in our rats provide a cogent explanation for the observed toxicity in our study: Cr was localized to the villi, which resulted in villous blunting and crypt proliferation. The overall similarity in histopathological effects observed in our rats with the effects observed in our mouse study (and NTP's mouse study) lead us to conclude that F344 rats might also develop intestinal tumors if they were to sustain chronic intestinal damage and regenerative proliferation. The synchrotron analyses indicated that Cr levels in the rat villi were ~2-fold lower than in the mouse villi; a similar 2-fold difference in Cr levels were reported in homogenized duodena from our studies (Kirman *et al.*, 2012; Thompson *et al.*, 2012b). Lower tissue doses in rats relative to mice in our studies, and lower water intake in the NTP rat studies relative to our rat study might explain why rats did not develop intestinal tumors in the NTP 2-year bioassay.

Tissue dosimetry explains the location of tumors in the mouse small intestine. In the mouse NTP 2-year bioassay, tumor induction at 180 mg/l Cr(VI) was highest in the duodenum, low in the jejunum, and nonexistent in the ileum and colon. At the second highest concentration (60 mg/l) there were no tumors beyond the duodenum. At the lowest study concentration (5 mg/l) there were no tumors in the intestine. Considering that crypts line the entire intestinal tract, the specificity of the tumor location is informative. First, Cr(VI) in the intestinal lumen can continue to be reduced to noncarcinogenic Cr(III) as it transits through the intestinal tract thereby limiting Cr(VI) exposure in distal regions. Second, the villi of the duodenum and proximal jejunum are where most nutrient absorption occurs, and thus where villus Cr(VI) absorption is likely highest. Consistent with tumor location and the aforementioned aspects on Cr(VI) reduction and absorption, we previously reported that Cr levels in homogenized intestinal sections from additional animals that were part of this study were highest in the duodenum, lower in the jejunum, and very low in the ileum (Kirman *et al.*, 2012; Thompson *et al.*, 2011, 2012b). The synchrotron analyses herein suggest that the majority of Cr that was measured in homogenized intestinal sections was localized to the villi. Intestinal crypts may be protected from Cr due to low transporter expression, as well as mucous secretions that limit chemical access to the crypt compartment (Cohen *et al.*, 2010; Greaves, 2012). Overall, the specificity of Cr(VI)-induced tumor formation to the proximal small intestine without apparent crypt exposure supports a nonlinear MOA wherein chronic exposure to high concentrations of Cr(VI) results in long-term villous wounding and regenerative crypt hyperplasia. At lower concentrations that do not induce chronic cytotoxicity, this MOA would not be operative.

The U.S. EPA regional screening level (RSL) of 0.035 μg/l for Cr(VI) in residential tap water has been proposed based on the assumption of a mutagenic MOA, that is, that the biology and risk of intestinal tumor formation from Cr(VI) exposure is linear (U.S. EPA, 2013). However, Cr(VI) concentrations in U.S. drinking water supplies range from 0.03 to 97 μg/l, with 73% of the source measurements being above the RSL (Supplementary Figure S6 and Supplementary Table S5). This implies that the majority of the water supplies in the United States pose an increased risk

for intestinal cancer. However, data in this present study indicate that such conservative linear extrapolations of risk for Cr(VI) exposure are unwarranted. DNA damage and Cr are minimally present if at all in the intestinal crypts of mice exposed to 180 000 μg/l Cr(VI); thus, risk to stem cells at lower environmental levels (<97 μg/l) is highly unlikely. Integration of the NTP study data and the mechanistic work described herein and elsewhere (Thompson *et al.*, 2013) support a non-mutagenic cytotoxic MOA that should be considered when assessing the carcinogenic risk of Cr(VI) in the intestine. In this regard, protection against intestinal hyperplasia should protect against Cr(VI)-induced intestinal carcinogenesis.

SUPPLEMENTARY DATA

Supplementary data are available online at http://toxsci.oxfordjournals.org/.

FUNDING

This work was supported by the Cr(VI) Panel of the American Chemistry Council.

Use of the NSLS (National Synchrotron Light Source) was supported by the DOE, Office of Science, Office of Basic Energy Sciences, under Contract No. DE-AC02-98CH10886.

ACKNOWLEDGMENTS

We thank Shelley Gruntz (EPL) for her assistance in preparation of tissue samples. The contents of this article reflect solely the view of the authors. Portions of this work were performed at Beamline X27A, National Synchrotron Light Source (NSLS), Brookhaven National Laboratory. X27A is supported in part by the U.S. Department of Energy (DOE)—Geosciences (DE-FG02-92ER14244 to The University of Chicago—CARS).

REFERENCES

Barker, N., Ridgway, R. A., van Es, J. H., van de Wetering, M., Begthel, H., van den Born, M., Danenberg, E., Clarke, A. R., Sansom, O. J., and Clevers, H. (2009). Crypt stem cells as the cells-of-origin of intestinal cancer. *Nature* **457**, 608–612.

Bonner, W. M., Redon, C. E., Dickey, J. S., Nakamura, A. J., Sedelnikova, O. A., Solier, S., and Pommier, Y. (2008). GammaH2AX and cancer. *Nat. Rev. Cancer* **8**, 957–967.

Cohen, S. M. (2010). An enhanced thirteen-week bioassay as an alternative for screening for carcinogenesis factors. *Asian Pac. J. Cancer Prev.* **11**, 15–17.

Cohen, S. M., Gordon, E. B., Singh, P., Arce, G. T., and Nyska, A. (2010). Carcinogenic mode of action of folpet in mice and evaluation of its relevance to humans. *Crit. Rev. Toxicol.* **40**, 531–545.

De Flora, S. (1978). Metabolic deactivation of mutagens in the Salmonella-microsome test. *Nature* **271**, 455–456.

De Flora, S., Camoirano, A., Bagnasco, M., Bennicelli, C., Corbett, G. E., and Kerger, B. D. (1997). Estimates of the chromium(VI) reducing capacity in human body compartments as a mechanism for attenuating its potential toxicity and carcinogenicity. *Carcinogenesis* **18**, 531–537.

DeSesso, J. M., and Jacobson, C. F. (2001). Anatomical and physiological parameters affecting gastrointestinal absorption in humans and rats. *Food Chem. Toxicol.* **39**, 209–228.

Ellis, A. S., Johnson, T. M., and Bullen, T. D. (2002). Chromium isotopes and the fate of hexavalent chromium in the environment. *Science* **295**, 2060–2062.

Gaylor, D. W. (2005). Are tumor incidence rates from chronic bioassays telling us what we need to know about carcinogens? *Regul. Toxicol. Pharmacol.* **41**, 128–133.

Gordon, E. (2007). Captan: Transition from 'B2' to 'not likely'. How pesticide registrants affected the EPA Cancer Classification Update. *J. Appl. Toxicol.* **27**, 519–526.

Greaves, P. (2012). *Histopathology of Preclinical Toxicity Studies* 4th ed. Elsevier-Academic Press, London.

Greenfield, R. E., Ellwein, L. B., and Cohen, S. M. (1984). A general probabilistic model of carcinogenesis: Analysis of experimental urinary bladder cancer. *Carcinogenesis* **5**, 437–445.

Hixon, G., and Bichteler, A. (2013). drsmooth: Dose-response modeling with smoothing splines. R package version 1.0. Available at: http://cran.r-project.org/web/packages/drsmooth/index.html. Accessed October 16, 2014.

Kinner, A., Wu, W., Staudt, C., and Iliakis, G. (2008). Gamma-H2AX in recognition and signaling of DNA double-strand breaks in the context of chromatin. *Nucleic Acids Res.* **36**, 5678–5694.

Kirman, C. R., Hays, S. M., Aylward, L. L., Suh, M., Harris, M. A., Thompson, C. M., Haws, L. C., and Proctor, D. M. (2012). Physiologically based pharmacokinetic model for rats and mice orally exposed to chromium. *Chem. Biol. Interact.* **200**, 45–64.

Kirman, C. R., Aylward, L. L., Suh, M., Harris, M. A., Thompson, C. M., Haws, L. C., Proctor, D. M., Lin, S. S., Parker, W., and Hays, S. M. (2013). Physiologically based pharmacokinetic model for humans orally exposed to chromium. *Chem. Biol. Interact.* **204**, 13–27.

Kopec, A. K., Kim, S., Forgacs, A. L., Zacharewski, T. R., Proctor, D. M., Harris, M. A., Haws, L. C., and Thompson, C. M. (2012). Genome-wide gene expression effects in B6C3F1 mouse intestinal epithelia following 7 and 90days of exposure to hexavalent chromium in drinking water. *Toxicol. Appl. Pharmacol.* **259**, 13–26.

Lanzirotti, L., and Sutton, S. (2002). Hard X-ray microprobe. *National Synchrotron Light Source*. Available at: http://www.bnl.gov/ps/nsls/newsroom/publications/otherpubs/imaging/hardxraymicroprobe.pdf. Accessed October 16, 2014.

Mackenzie, R. D., Byerrum, R. U., Decker, C. F., Hoppert, C. A., and Langham, R. F. (1958). Chronic toxicity studies. II. Hexavalent and trivalent chromium administered in drinking water to rats. *AMA Arch. Ind. Health* **18**, 232–234.

McCarroll, N., Keshava, N., Chen, J., Akerman, G., Kligerman, A., and Rinde, E. (2010). An evaluation of the mode of action framework for mutagenic carcinogens case study II: Chromium (VI). *Environ. Mol. Mutagen.* **51**, 89–111.

McNeill, L. S., Mclean, J. E., Parks, J. L., and Edwards, M. A. (2012). Hexavalent chromium review, part 2: Chemistry, occurrence, and treatment. *J. Am. Waterworks Assoc.* **104**, E395–E405.

Moolgavkar, S. H., and Knudson, A. G., Jr. (1981). Mutation and cancer: A model for human carcinogenesis. *J. Natl Cancer Inst.* **66**, 1037–1052.

Nickens, K. P., Patierno, S. R., and Ceryak, S. (2010). Chromium genotoxicity: A double-edged sword. *Chem. Biol. Interact.* **188**, 276–288.

NTP (2007). National Toxicology Program technical report on the toxicity studies of sodium dichromate dihydrate (CAS No. 7789-12-0) administered in drinking water to male and female F344/N rats and B6C3F1 mice and male BALB/c and *am3*-C57BL/6 mice. *NTP Toxicity Report Series Number 72, NIH Publication No.* 07-5964.

NTP (2008a). National Toxicology Program technical report on the toxicology and carcinogenesis studies of chromium picolinate monohydrate (CAS NO. 27882-76-4) in F344/N rats and B6C3F1 mice (feed studies). *NIH Publication No.* 08-5897.

NTP (2008b). National Toxicology Program technical report on the toxicology and carcinogenesis studies of sodium dichromate dihydrate (CAS No. 7789-12-0) in F344/N rats and B6C3F1 mice (drinking water studies), NTP TR 546. *NIH Publication No*. 08-5887.

O'Brien, T. J., Ceryak, S., and Patierno, S. R. (2003). Complexities of chromium carcinogenesis: Role of cellular response, repair and recovery mechanisms. *Mutat. Res.* **533**, 3–36.

O'Brien, T. J., Ding, H., Suh, M., Thompson, C. M., Parsons, B. L., Harris, M. A., Winkelman, W. A., Wolf, J. C., Hixon, J. G., Schwartz, A. M., Myers, M. B., Haws, L. C., and Proctor, D. M. (2013). Assessment of K-Ras mutant frequency and micronucleus incidence in the mouse duodenum following 90-days of exposure to Cr(VI) in drinking water. *Mutat. Res.* **754**, 15–21.

OEHHA (2011). Final technical support document on public health goal for hexavalent chromium in drinking water. *Pesticide and Environmental Toxicology Branch, Office of Environmental Health Hazard Assessment, California Environmental Protection Agency*.

Oze, C., Bird, D. K., and Fendorf, S. (2007). Genesis of hexavalent chromium from natural sources in soil and groundwater. *Proc. Natl Acad. Sci. USA* **104**, 6544–6549.

Potten, C. S., and Loeffler, M. (1990). Stem cells: Attributes, cycles, spirals, pitfalls and uncertainties. Lessons for and from the crypt. *Development* **110**, 1001–1020.

Proctor, D. M., Suh, M., Aylward, L. L., Kirman, C. R., Harris, M. A., Thompson, C. M., Gurleyuk, H., Gerads, R., Haws, L. C., and Hays, S. M. (2012). Hexavalent chromium reduction kinetics in rodent stomach contents. *Chemosphere* **89**, 487–493.

Rizk, P., and Barker, N. (2012). Gut stem cells in tissue renewal and disease: Methods, markers, and myths. *Wiley interdisciplinary reviews. Sys. Biol. Med.* **4**, 475–496.

Rousseau, R. M. (2001). Detection limit and estimate of uncertainty of analytical XRF results. *Rigaku* **18**, 33–47.

Schuijers, J., and Clevers, H. (2012). Adult mammalian stem cells: The role of Wnt, Lgr5 and R-spondins. *Embo J.* **31**, 3031–3032.

Schwitalla, S., Fingerle, A. A., Cammareri, P., Nebelsiek, T., Goktuna, S. I., Ziegler, P. K., Canli, O., Heijmans, J., Huels, D. J., Moreaux, G., *et al.* (2013). Intestinal tumorigenesis initiated by dedifferentiation and acquisition of stem-cell-like properties. *Cell* **152**, 25–38.

Stout, M. D., Herbert, R. A., Kissling, G. E., Collins, B. J., Travlos, G. S., Witt, K. L., Melnick, R. L., Abdo, K. M., Malarkey, D. E., and Hooth, M. J. (2009a). Hexavalent chromium is carcinogenic to F344/N rats and B6C3F1 mice after chronic oral exposure. *Environ. Health Perspect.* **117**, 716–722.

Stout, M. D., Nyska, A., Collins, B. J., Witt, K. L., Kissling, G. E., Malarkey, D. E., and Hooth, M. J. (2009b). Chronic toxicity and carcinogenicity studies of chromium picolinate monohydrate administered in feed to F344/N rats and B6C3F1 mice for 2 years. *Food Chem. Toxicol.* **47**, 729–733.

Thompson, C. M., Proctor, D. M., Haws, L. C., Hebert, C. D., Grimes, S. D., Shertzer, H. G., Kopec, A. K., Hixon, J. G., Zacharewski, T. R., and Harris, M. A. (2011). Investigation of the mode of action underlying the tumorigenic response induced in B6C3F1 mice exposed orally to hexavalent chromium. *Toxicol. Sci.* **123**, 58–70.

Thompson, C. M., Fedorov, Y., D., B. D., Suh, M., Proctor, D. M., Kuriakose, L., Haws, L. C., and Harris, M. A. (2012a). Assessment of Cr(VI)-induced cytotoxicity and genotoxicity using high content analysis. *PLoS One* **7**, e42720.

Thompson, C. M., Proctor, D. M., Suh, M., Haws, L. C., Hebert, C. D., Mann, J. F., Shertzer, H. G., Hixon, J. G., and Harris, M. A. (2012b). Comparison of the effects of hexavalent chromium in the alimentary canal of F344 rats and B6C3F1 mice following exposure in drinking water: Implications for carcinogenic modes of action. *Toxicol. Sci.* **125**, 79–90.

Thompson, C. M., Proctor, D. M., Suh, M., Haws, L. C., Kirman, C. R., and Harris, M. A. (2013). Assessment of the mode of action underlying development of rodent small intestinal tumors following oral exposure to hexavalent chromium and relevance to humans. *Crit. Rev. Toxicol.* **43**, 244–274.

U.S. EPA (1991). National primary drinking water regulations-synthetic organic chemicals and inorganic chemicals; monitoring for unregulated contaminants; national primary drinking water regulations implementation; national secondary drinking water regulations. Final rule. *Fed. Reg.* **56**, 3526–3597.

U.S. Environmental Protection Agency (EPA) (1998). Toxicological review of hexavalent chromium in support of summary information on the integrated risk information system (IRIS). *U.S. Environmental Protection Agency, Washinton, D.C.*

U.S. EPA (2004). Captan; cancer reclassification; Amendment of reregistration eligibility decision; notice of availability. *Fed. Reg.* **69**, 68357–68360.

U.S. EPA (2013). Regional Screening Levels. Available at: http://www.epa.gov/region9/superfund/prg/. Accessed October 16, 2014.

U.S. EPA (2014). The Third Unregulated Contaminant Monitoring Rule (UCMR3): Occurrence Data. Available at: http://water.epa.gov/lawsregs/rulesregs/sdwa/ucmr/data.cfm. Accessed August 14, 2014.

van der Flier, L. G., and Clevers, H. (2009). Stem cells, self-renewal, and differentiation in the intestinal epithelium. *Annu. Rev. Physiol.* **71**, 241–260.

Zhitkovich, A. (2011). Chromium in drinking water: Sources, metabolism, and cancer risks. *Chem. Res. Toxicol.* **24**, 1617–1629.